The low-temperature phase sequence gamma - delta - epsilon in halide perovskite tetramethylammonium trichlorogermanate(II) studied by X-ray diffraction

1995 J. Phys.: Condens. Matter 7 4983

(http://iopscience.iop.org/0953-8984/7/26/005)

J. Phys.: Condens. Matter 7 (1995) 4983–4998. Printed in the UK

The low-temperature phase sequence γ–δ–ε in halide perovskite tetramethylammonium trichlorogermanate(II) studied by x-ray diffraction

Klaus Fütterer†‡§, Ray L Withers†, T R Welberry† and Wulf Depmeier‡

† Research School of Chemistry, Australian National University, Canberra ACT 0200, Australia
‡ Mineralogisch-Petrographisches Institut, Christian-Albrechts-Universität zu Kiel, D-24098 Kiel, Germany

Received 7 March 1995

Abstract. The halide perovskite tetramethylammonium trichlorogermanate(II), $N(CH_3)_4GeCl_3$, undergoes a structural phase transition at 200 K from an orthorhombic room-temperature phase to an incommensurately modulated orthorhombic phase and at 170 K a further transition to a phase characterized by the coexistence of a monoclinic and an orthorhombic Bravais lattice. It is proposed that the superposition of the two Bravais lattices results from the low bulk modulus (9 GPa) in conjunction with the formation of ferroelastic domains. Local stresses implied by adjacent monoclinic domains allow the soft material to form orthorhombic domain boundaries. Two order parameters ξ and η governing the phase transition at 170 K can be related to a translational and a rotational part of the displacive modulation of the rigid $GeCl_3$ and tetramethylammonium molecules. Experimental evidence suggests that the displacive modulation in the incommensurate phase is related to short-range disorder observed in the room-temperature phase.

1. Introduction

Tetramethylammonium trichlorogermanate(II), $N(CH_3)_4GeCl_3$ (TGC for short), is a member of the family of halide perovskite compounds with general formula AMX_3 ($A = Rb^+, Cs^+, NH_{4-x}(CH_3)_x, \ldots$; $M = Ge^{2+}, Sn^{2+}, Pb^{2+}$ and $X = Cl^-, Br^-, I^-$). A common feature of this series of compounds is the subvalent metal ion resulting in an electron lone pair. Many of these compounds exhibit a cubic high-temperature phase, which is often but not necessarily isomorphous to the perovskite structure. In the case of the germanate compounds, the transition into the cubic phase typically takes place at about 450 K and is associated with the onset of a high ionic conductivity due to the halide ions becoming mobile (Yamada *et al* 1994).

TGC is orthorhombic at room temperature (γ-phase), space group *Pnam* (Hesse *et al* 1995, Yamada *et al* 1994), with $a = 13.11$ Å, $b = 8.95$ Å, $c = 9.14$ Å. A schematic representation of the phase transition sequence as a function of temperature is depicted in figure 1. It shows the five phases so far known of TGC. The transition temperatures in figure 1 refer to DSC (Möller 1980) and ^{35}Cl NQR measurements (Yamada *et al* 1994). The so-called β-phase (390 K $< T <$ 428 K), which is intermediate between the cubic high-temperature

§ Present address: Department of Biochemistry and Molecular Biophysics, Washington University School of Medicine, Box 8231, 660 South Euclid Avenue, St Louis, MO, 63110, USA.

0953-8984/95/264983+16$19.50

428 K	α-Phase	$Pm\bar{3}m$	6.55 Å
390 K	β-Phase	?	?
200 K	γ-Phase	*Pnam*	13.08 x 8.89 x 9.12 Å^3
170 K	δ-Phase	*Pnam(0β0)00s*	13.08 x 8.84 x9.03 Å^3
	ε-Phase	$P2_1/n11$ $Pna2_1$	13.03 x 8.79 x 8.91 Å^3, α = 94.7° 13.03 x 8.79 x 8.96 Å^3

Figure 1. Phases of TGC as a function of temperature.

and the orthorhombic room-temperature phase, has to date only been observed by DSC (Möller 1980). DSC results (Möller 1980) also gave the first evidence for the occurrence of two further low-temperature phase transitions into the so-called δ- and ε-phases. The existence of these two phase transitions was later confirmed by ^{35}Cl NQR (Yamada *et al* 1994). X-ray powder and single-crystal diffraction revealed the δ-phase to be orthorhombic and incommensurately modulated. The ε-phase was shown to be non-modulated. The intriguing feature of the ε-phase is the coexistence of a monoclinic and an orthorhombic lattice persisting from $T_{\delta-\varepsilon} = 170$ K down to at least $T = 130$ K, i.e. the lower limit of our experimental investigations (Fütterer *et al* 1995).

Whilst the focus of Fütterer *et al* (1995) was predominantly on the modulated structure of the incommensurate phase and gave only a preliminary description of the low-temperature phase transition sequence, this paper presents in detail the results of our low-temperature x-ray study on TGC. An attempt is made to understand the phase transition sequence and the occurrence of two superimposing lattices in the ε-phase via a phenomenological Landau theory approach.

2. Experimental details

2.1. Synthesis

Crystals suitable for x-ray structure investigation were grown by a convection method following a procedure given by Möller (1980), from an equimolar solution of $N(CH_3)_4Cl$ and $GeCl_2$ in 5 M HCl. Guinier and precession photographs identified the sample and confirmed its purity.

2.2. X-ray diffraction

2.2.1. Powder diffraction. Temperature-dependent powder diffraction patterns were recorded on a Guinier x-ray diffractometer in steps of 10 K between 300 K and 130 K and on a finer scale, i.e. $\Delta T = 2$ K, for 160 K $< T <$ 220 K. For this measurement a Huber G645 diffractometer was used with an attached helium closed cycle cooling stage (CTI Cryogenics 22C).

2.2.2. Single-crystal diffraction. Buerger precession photographs of reciprocal lattice layers $h, k, (0, 1, 2)$ and $(0, 1, 2), k, l$ (indices refer to the γ-TGC reciprocal lattice) were recorded at room temperature as well as at 183 K and 158 K, using a nitrogen flow cooling stage (Leybold-Heraeus, TCD 1) and Zr-filtered Mo radiation.

The single-crystal data were recorded on a Stoe–Siemens four-circle diffractometer equipped with a cold-nitrogen flow cooling device (Oxford Cryosystems Cryostream). Mo Kα radiation was used (pyrolytic graphite(111) monochromator).

2.2.3. Determination of the modulation wave vector. The modulus of the modulation wave vector $q = \delta b^*$ characteristic of the δ-phase was determined from the peak–peak distance of satellite reflections $hklm$ and $hkl\bar{m}$ obtained by performing Q scans along b^*. This procedure allowed δ to be determined up to ± 0.001. The temperature dependence of δ was measured in the interval 170 K $\leqslant T \leqslant$ 200 K in variable steps of 2.5 K down to 1 K by determining the peak–peak distance of reflections $006m$ and $006\bar{m}$, $m = 1, 2, 3$.

2.3. Diffuse x-ray scattering

Diffuse x-ray scattering was measured on a special diffractometer described elsewhere (Osborn and Welberry 1990) using a one-dimensional position sensitive detector. A crystal of approximate dimensions Ø0.4 mm × 0.6 mm was mounted along the [100] direction. A diffuse scattering pattern of the $0kl$ reciprocal lattice plane was then recorded at room temperature.

3. Experimental observations

3.1. In the γ-phase

(1) Unusually high atomic thermal parameters U_{ii} result from the structure refinement of TGC in the γ-phase (Hesse *et al* 1995). U_{33} is observed to be in general distinctly higher than the two other components, those being of about the same magnitude for the Ge and Cl atoms. Figure 2, adapted from those authors, displays the temperature dependence of the average of U_{ii} of the $GeCl_3$ anion and the TMA cation, respectively, where the average was weighted by the number of electrons. Whilst linear extrapolation of U_{11}, U_{22} to $T = 0$ leads to $U_{11} = U_{22} \approx 0$, U_{33} behaves abnormally in extrapolating to values distinctly different from zero for $T \to 0$.

(2) The lattice parameters decrease linearly on cooling with the slopes being $\partial a/\partial T = (3.4 \pm 0.1) \times 10^{-4}$, $\partial b/\partial T = (7.5 \pm 0.1) \times 10^{-4}$, $\partial c/\partial T = (1.08 \pm 0.1) \times 10^{-3}$ (see figure 3).

(3) Superimposed on the Bragg reflections in the $0kl$ reciprocal plane are diffuse streaks of scattered x-ray intensity (see figure 4). The streaks are oriented perpendicular to the corresponding reciprocal axis for reflections $00l$ and $0k0$, respectively. They display a bow-tie-shape for reflections $0, \pm k, \pm k$ and intermediate shapes between bow-tie and straight streaks for general reflections $0kl$.

3.2. At the γ–δ transition

(1) Below $T_{\gamma-\delta} = 200$ K $\pm$ 2 K satellite reflections occur at $mq = m\delta b^*$, with $\delta = 0.140(1)$ at 190 K and m an integer. They increase in intensity with decreasing temperature as displayed in figure 5.

(2) The intensity evolution of the main reflection 006 across the γ–δ transition is continuous. The transition is marked by a kink in the slope $\partial I/\partial T$ (see figure 6). Below $T_{\gamma-\delta}$, $I(006)$ shows a rapid decrease with decreasing temperature. Simultaneously, the intensities of satellite reflections 0061 and 0062 increase with decreasing temperature as displayed in figure 5.

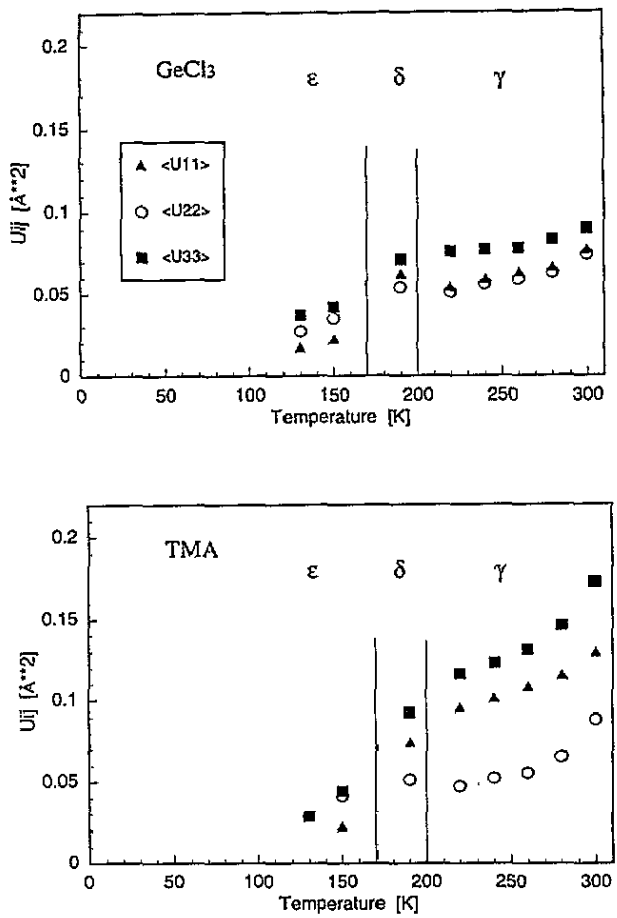

Figure 2. Temperature dependence of the averaged thermal parameter tensor components $U_{ii}, i = 1, 2, 3$ for the $GeCl_3^-$ and the TMA^+ ion, respectively. The average is weighted by the number of electrons comprised within the corresponding molecule. (Figure received as personal communication from Hesse *et al* (1995).)

(3) The evolution of lattice parameters with decreasing temperature displays a kink at $T_{\gamma-\delta}$. Whilst $b(T)$ and $c(T)$ exhibit an increase of the slope to $\partial b/\partial T = (1.10 \pm 0.02) \times 10^{-3}$ and $\partial c/\partial T = (1.42 \pm 0.04) \times 10^{-3}$, respectively, the slope of $a(T)$ becomes nearly zero, i.e. $\partial a/\partial T = (6.2 \pm 3.0) \times 10^{-5}$, below the γ–δ phase transition (see figure 3, cf. item (2) in 3.1).

3.3. In the δ-phase

(1) The satellite reflections were observed by single-crystal as well as by powder diffraction.

(2) The superspace group $Pnam(0\beta0)00s$ complies with the systematic extinction conditions observed in the δ-phase. The refinement of the modulated structure in superspace group $Pnam(0\beta0)00s$ at 190 K (Fütterer *et al* 1995) revealed a displacive modulation wave predominantly polarized along the c axis with an amplitude of ~0.4 Å magnitude. Displacements along a or b exceeding 0.1 Å were only observed for two of the three

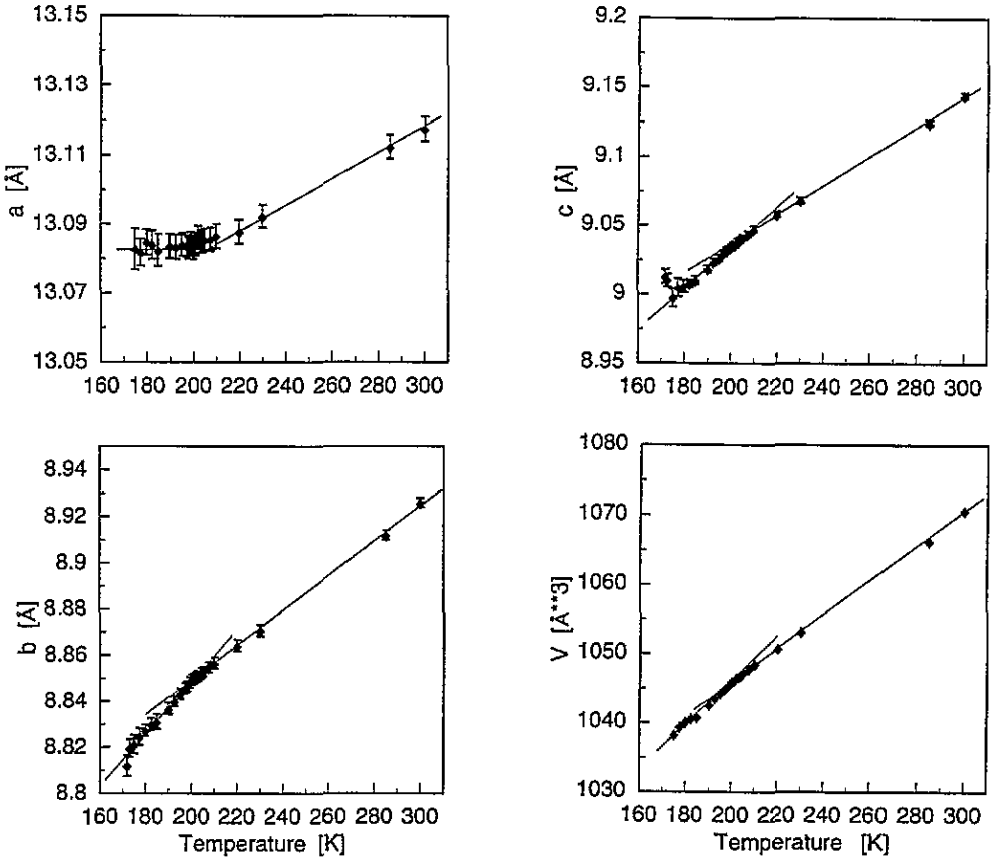

Figure 3. Lattice parameters as a function of temperature. The γ–δ transition at 200 K is marked by a distinct change of slope.

symmetrically independent carbon atoms of the TMA cation.

(3) The temperature dependence of q is continuous with $0.11b^* \leqslant q \leqslant 0.14b^*$ for 170 K $< T <$ 200 K (see figure 7).

3.4. At the δ–ε transition

(1) The precession photograph of the $0kl$ layer shows two monoclinic reciprocal lattices (related by twinning) as well as an orthorhombic reciprocal lattice, whereas the $hk0$ layer is unaltered compared to the δ- and γ-phase.

(2) The peak splittings observed in the powder diffraction pattern could also be interpreted as resulting from the superposition of an orthorhombic and a monoclinic lattice.

(3) The satellite reflections disappear at the transition (see figure 5). Note that the monoclinic reflections overlap with disappearing satellites of third order in the case of 0063, of second order in the case of 0042 and of first order for 0021, respectively. However, the positions of monoclinic main reflections and orthorhombic satellites, respectively, can be distinguished by means of Q scans on the four-circle diffractometer. This becomes apparent when determining the peak–peak distance of satellite reflections, because the values of δ (defined by $q = \delta b^*$), as determined from disappearing satellites and from 'satellites', which become strong (i.e. are in fact monoclinic main reflections), differ by more than 5σ of the

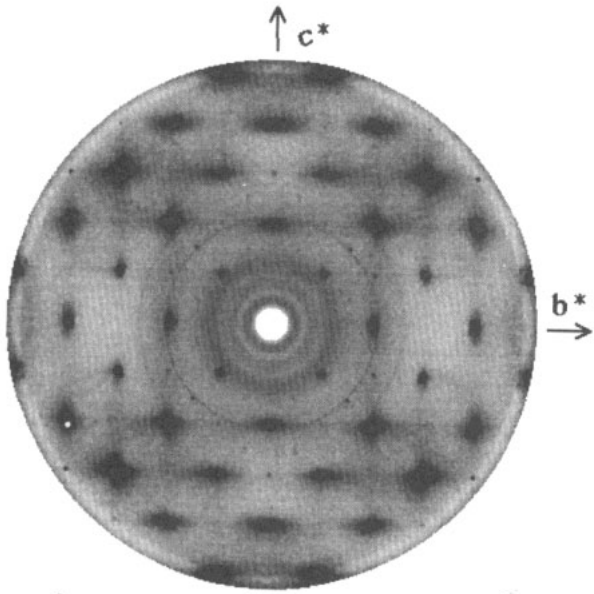

Figure 4. Diffuse scattering pattern of TGC at room temperature in reciprocal plane $0kl$.

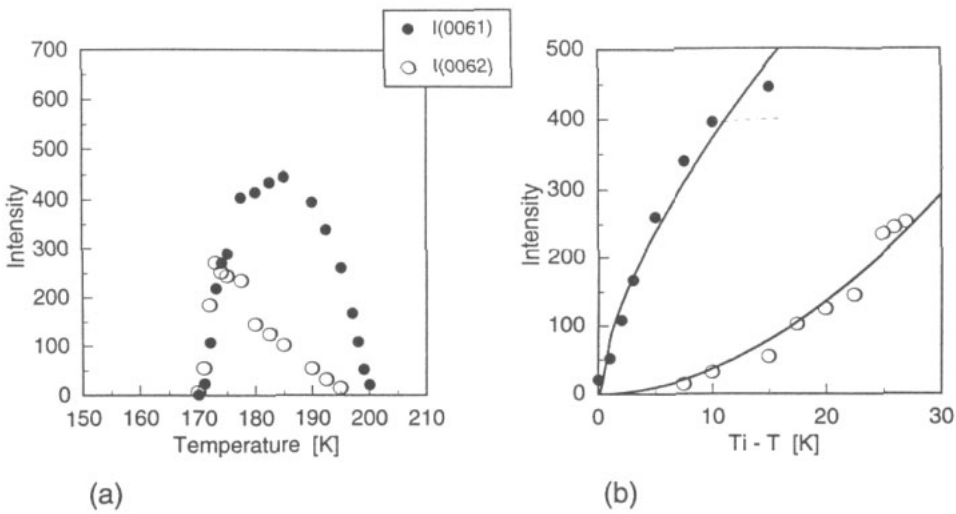

Figure 5. (a) Intensity of reflections 0061 and 0062 as a function of temperature. (b) Intensity of the same reflections plotted against. $(T_{\gamma-\delta} - T)$ with $T_{\gamma-\delta} = 200$ K. The solid curves represent a least squares fit of the data to the function $y = a(T_{\gamma-\delta} - T)^{\beta}$.

experimental uncertainty (cf. 2.2).

(4) The intensity of reflections $00l_{\mathrm{mcl}}$ and $00l_{\mathrm{ort}}$ shows a steep (if not steplike) increase with decreasing temperature at the δ–ε transition (see figure 6).

(5) A thermal hysteresis of about 8 K is observed. The apparent overlap of the δ- and ε-phase is an experimental artefact due to the experimental uncertainty in determining $T_{\delta-\varepsilon} = 172 \pm 2$ K.

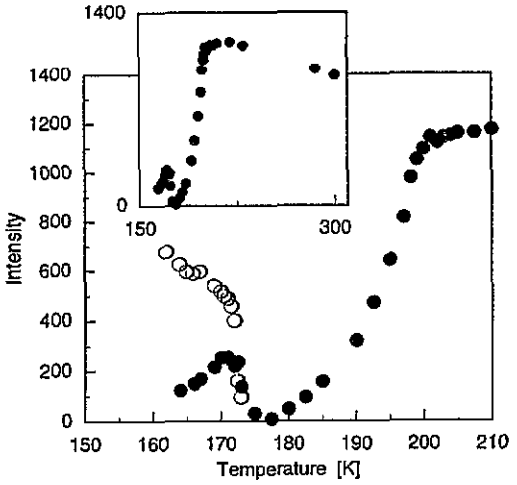

Figure 6. Intensity of main reflections 006_o (closed circles) and 006_m (open circles) as a function of temperature, where the subscripts refer to the orthorhombic and the monoclinic reflections, respectively. The inset shows the evolution of 006_o over the whole temperature range of the experiment.

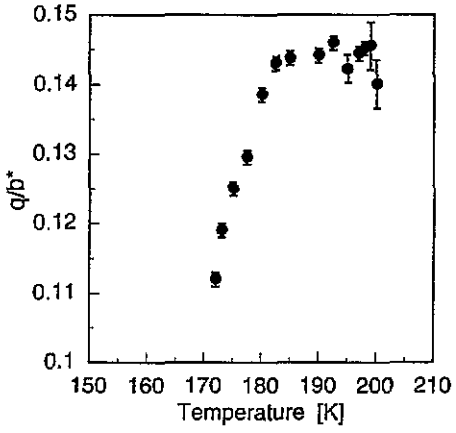

Figure 7. Modulation wave vector $q = \delta b^*$ as a function of temperature.

3.5. In the ε-phase

(1) The lattice parameters as determined from a powder diffraction pattern recorded at 160 K were 13.046(6) × 8.788(5) × 8.99(1) Å^3 and 13.068(6) × 8.808(5) × 8.962(6) Å^3, $\alpha = 93.9(1)°$ for the orthorhombic and the monoclinic lattice, respectively. The lattice parameters were also determined from the precession exposures recorded at 158 K and the result was 13.03(1)×8.79(1)×8.96(1) Å^3 and 13.03(1)×8.79(1)×8.91(1) Å^3, $\alpha = 94.7(1)°$ for the orthorhombic and monoclinic case, respectively.

(2) The systematic extinction conditions observed in the $0kl$ layer recorded in the ε-phase are, for both lattices, $F(0kl) = 0$ unless $k + l = 2n$. The layer $hk0$ shows the extinction conditions $F(h00) = 0$ unless $h = 2n$ and $F(0k0) = 0$ unless $k = 2n$, again for both lattices. From the higher-level exposures, i.e. $1kl$, $2kl$ and $hk1$, $hk2$, the extinction condition $F(h0l) = 0$ unless $h = 2n$ became apparent for the orthorhombic lattice.

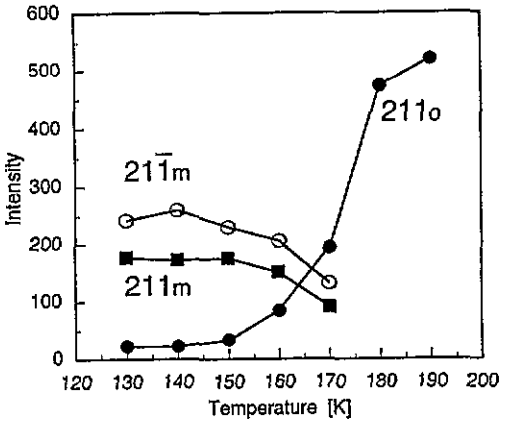

Figure 8. Temperature dependence of the intensity of reflections 211_o (orthorhombic) and 211_m, $21\bar{1}_m$ (monoclinic) as observed by powder diffraction across the δ–ε phase transition.

(3) The intensity ratio of orthorhombic and monoclinic reflections was observed to vary from sample to sample. It is essentially constant below 150 K (see figure 8). A complete transformation to the monoclinic phase, i.e. the disappearance of the intensity of the orthorhombic reflections, was not observed. However, experiments have only been carried out to a lower temperature limit of 130 K.

4. Discussion

4.1. Characteristic features of the modulated phase

The temperature dependence of the primary modulation wave vector $q = \delta b^*$ is displayed in figure 7. The continuous variation of δ with T indicates that q is incommensurate rather than commensurate. The characteristic feature is the plateau at $\delta \approx \frac{1}{7}$ for 200 K > T > 180 K and the steep, but smooth descent to $\delta \approx \frac{1}{9}$ below 180 K. Such a behaviour is commonly attributed to two different regimes of an incommensurate phase, the so-called sinusoidal and soliton regimes, respectively (see Levanyuk 1986). As long as the modulation wave can be described by a plane wave approximation, q does not change. With increasing amplitude, however, the harmonic wave becomes increasingly distorted, which is reflected by the fact that the order of observable satellite reflections increases. Indeed, satellite reflections up to fourth order can be observed right above the δ–ε transition, whereas only first-order ones are observed right below the γ–δ transition. The incommensurate phase is then rather to be described by a pattern of commensurate domains separated by incommensurate domain walls, the latter often called discommensurations or solitons. Those domain walls interact with each other, depending on the density of domains (see Salje 1990). The latter quantity is temperature dependent, and therefore q is varying with temperature as well, once the soliton regime is reached.

The increase of the intensities of satellite reflections 0061 and 0062 (see figure 5) below $T_{\gamma-\delta}$ exhibits a behaviour, which was also found in some of the A_2BX_4 compounds. For those compounds Majkrzak *et al* (1980) derived the functional dependence $I_{1,2} = B_{1,2}(T_i - T)^{\beta_{1,2}}$ for the temperature-dependent behaviour of first- and second-order satellites, which was based on the XY-model of ferromagnetism and where T_i is the normal–incommensurate transition temperature. The critical exponents for the increasing intensity

below T_i obtained from this model are $\beta_1 = 0.70(4)$ and $\beta_2 = 1.69(9)$ for the first- and second-order satellites, respectively. The corresponding values for TGC are $\beta_1 = 0.64(7)$ and $\beta_2 = 1.75(7)$. This is to be compared with $\beta_1 = 0.75(5)$ and $\beta_2 = 1.57(7)$ (K_2SeO_4; Majkrzak *et al* 1980), and $\beta_1 = 0.75(5)$ (Rb_2ZnCl_4; Mashiyama 1981). Within error TGC apparently follows closely the behaviour known from the A_2BX_4 compounds.

4.2. The superposition of two Bravais lattices

The occurrence of the superposition of two different Bravais lattices is a surprising peculiarity of TGC, but not really an uncommon phenomenon. There are other compounds, where analogous observations have been made. Pb_2CoWO_6 shows similar characteristics (Sciau *et al* 1992, Rabe and Schmid 1993). However, experimental results have to be carefully checked with regard to a possible artefact.

Several aspects make us confident to trust our results. Firstly, the superposition of two different, reciprocal Bravais lattices is observed by both powder and single-crystal diffraction (items (1) and (2) in subsection 3.4). Secondly, the lattice parameters obtained from powder diffraction and from the precession photographs are in close agreement (item (1), Sn 3.5), supporting the assumption that the same effect was observed in both cases. Thirdly, as will be demonstrated in section 4.3, symmetry allows both lattices to occur as subgroups of *Pnam*.

The superposition persists down to at least 130 K and was observed to occur for all samples and independently from different cooling rates. Its presence seems to be also independent from the thermal hysteresis of about 8 K observed at the δ–ε transition (item (5), Sn 3.4). Furthermore, the satellite reflections apparently disappear completely at the δ–ε transition and are not only lowered in intensity. This suggests that the superposition is a genuine property of the ε-phase, and that we do not observe an overlap of the δ- with the ε-phase.

As ferroelastic phase transitions inevitably imply twinning of the crystal, often resulting in domains visible under polarized light, we carried out a preliminary polarized light microscopy study on TGC single crystals at low temperature. Below the δ–ε transition a striped state of the crystal became visible, with the stripes being about 10 to 20 μm wide in about 250 μm-sized single crystals. The stripe boundaries appeared to be diffuse rather than sharp. Once the striped state became visible, the density and orientation of domains did not change notably any more.

These observations, though being of preliminary character, might be cautiously interpreted by attributing the stripes to ferroelastic monoclinic domains occurring due to the orthorhombic $\rightarrow$ monoclinic phase transition. The low bulk modulus of 9 GPa (Fütterer 1994) indicates that TGC is a very soft material. Thus, it is conceivable that the coexisting orthorhombic Bravais lattice results from the domain boundary regions. Local stress imposed by adjacent monoclinic domains might well result in a smooth transition from one monoclinic domain to the next and, therefore, on average in an orthorhombic lattice in the area of the domain wall. Other authors have considered e.g. chemical exsolution as the origin for such a superposition, as was argued in the case of $(Pb_{1-x}B_x)_3(PO_4)_2$ (Hensler *et al* 1993). Although an exsolution process cannot be definitely excluded, it is highly unlikely, since TGC, unlike $(Pb_{1-x}B_x)_3(PO_4)_2$, is not a solid solution.

4.3. Phenomenological description

Following the approach of Levanyuk and Sannikov (1976) for a phenomenological description of the γ–δ–ε phase transition sequence, we are considering the phases γ and ε as parent and low-symmetry phases respectively. The intermediate incommensurate phase δ is taken into account by allowing for a spatial variation of the order parameter. Since the γ- and ε-phases are equitranslational, i.e. $q = 0$, the (virtual) γ–ε transition takes place at the centre of the Brillouin zone and the irreducible representations governing the symmetry properties of the transition are one dimensional. Consequently, the order parameter, in terms of which the Landau free energy potential is to be expanded, is one dimensional as well and a Lifshitz invariant can not exist. However, as in the case of $NaNO_2$, thiourea (Levanyuk and Sannikov 1976) or quartz (Dolino 1986) the Landau potential may be expanded in terms of two independent order parameters. They obey two different irreducible representations and interact via a gradient coupling term, called a Lifshitz-*like* invariant.

Table 1. Irreducible representations of *Pnam* with $q = 0$, calculated with the computer program KAREP.

	$\{E\|0\}$	$\{C_{2y}\|\frac{1}{2}(ab)\}$	$\{\sigma_x\|\frac{1}{2}(a+b+c)\}$	$\{\sigma_z\|\frac{1}{2}c\}$	$\{I\|0\}$	$\{C_{2x}\|\frac{1}{2}(a+b+c)\}$	$\{C_{2z}\|\frac{1}{2}c\}$	$\{\sigma_y\|\frac{1}{2}(a+b)\}$
Γ_1	1	1	1	1	1	1	1	1
Γ_2	1	1	−1	−1	−1	1	1	−1
Γ_3	1	1	−1	−1	1	−1	−1	1
Γ_4	1	1	1	1	−1	−1	−1	−1
Γ_5	1	−1	−1	1	1	−1	1	−1
Γ_6	1	−1	1	−1	−1	−1	1	1
Γ_7	1	−1	1	−1	1	1	−1	−1
Γ_8	1	−1	−1	1	−1	1	−1	1

In table 1 the irreducible representations of *Pnam* for the Γ point of the Brillouin zone are listed (calculated using the computer program KAREP, Hovestreydt *et al* 1992). The Landau potential is written according to Levanyuk and Sannikov (1976) as follows:

$$\Phi = \frac{\alpha}{2}\xi^2 + \frac{\alpha'}{2}\eta^2 + \frac{\beta}{4}\xi^4 + \frac{\beta'}{4}\eta^4 + \frac{\sigma}{2}\left(\eta\,\partial_y\xi - \xi\,\partial_y\eta\right) + \frac{\zeta}{2}\left(\partial_y\xi\right)^2 + \frac{\zeta'}{2}\left(\partial_y\eta\right)^2. \qquad (1)$$

Here, α is temperature dependent and α', β, β', ζ, ζ' are assumed to be positive. The first order parameter ξ transforms according to Γ_7, while the second order parameter η transforms according to Γ_6. The two order parameters can be related to a translational and coupled rotational distortion mode of the parent structure, as will be outlined later on. The interaction of the two order parameters is mediated by the σ term, which is the Lifshitz-like invariant.

Minimizing the free energy with respect to ξ and η leads to two differential equations (Levanyuk and Sannikov 1976). Apart from the trivial solutions $\xi = \eta = 0$ representing the parent phase, there are at least two other solutions, i.e.

$$\xi = \rho\cos q\cdot r,\ \eta = \rho'\sin q\cdot r \qquad \xi = \xi_s,\ \eta = 0.$$

The second solution describes the incommensurate phase, i.e. the δ-phase, whereas the third one represents the low-symmetry phase ε (for a detailed discussion of those solutions see Levanyuk and Sannikov 1976).

While the order parameter ξ associated with the representation Γ_7 would lead to $P2_1/n11$ symmetry of the low-symmetry phase, the order parameter η associated with Γ_6 would lead to $Pna2_1$. Thus the third solution would suggest the ε-phase to be monoclinic

and the orthorhombic part to disappear, in contradiction to the experimental observation of both symmetries. However, the assumption of α' being independent from temperature is likely oversimplified. Moreover, the form of the chosen potential equally allows the choice of α' to be temperature dependent and α to be positive, which would then lead to the opposite result $\xi = 0$, $\eta = \eta_s$. Therefore, it is quite plausible to assume that the occurrence of either the monoclinic or the orthorhombic part depends on the actual values of the expansion coefficients, but symmetry does not exclude either of them.

The same result is obtained when considering the lock in of the atomic modulation functions (AMF) in the δ-phase for $q \to 0$. To lock in the incommensurate structure at a commensurate value of q, we can require either the inversion or the glide plane perpendicular to b to be a symmetry operation. This choice fixes the origin of $q \cdot t$ and results in different three-dimensional space groups of the locked-in phase, as will be shown below.

Let $u(t, \mu) = \Re Q_q e(q, \mu) e^{2\pi q \cdot t}$ represent the AMF, which describes the pattern of atomic displacements in the incommensurate phase with the modulation wave vector $q = \delta b^*$. Here Q_q is a complex order parameter, $e(q, \mu)$ a complex eigenvector and $e^{2\pi q \cdot t}$ describes the spatial dependence of the displacements with t being a Bravais lattice vector. We restrict ourselves to considering the first-order harmonic displacement, which in superspace group $Pnam(0\beta0)00s$ allows only c axis 'motion' for atoms situated on the m_z mirror plane. Let $Ge_1, \ldots, Ge_4$ denote the four symmetrically equivalent Ge atoms in the unit cell of the average structure. The eigenvector representing these four atoms reads

$$\begin{aligned} e(q) &= (0, 0, e_z(Ge_1)|0, 0, e_z(Ge_2)|0, 0, e_z(Ge_3)|0, 0, e_z(Ge_4)) \\ &= (0, 0, e_z(Ge_1)|0, 0, e_z(Ge_1)e^{i\pi\delta}|0, 0, e_z(Ge_3)|0, 0, e_z(Ge_3)e^{i\pi\delta}) \end{aligned}$$

with Ge_1 at $(0.2571, 0.2517, \frac{3}{4})$ (Fütterer *et al* 1995) and

$$\begin{aligned} \{\sigma_x|\tfrac{1}{2}(a+b+c)\}Ge_1 \to Ge_2 \qquad & e_z(Ge_1) = e_z(Ge_2)e^{-i\pi\delta} \\ \{\sigma_x|\tfrac{1}{2}(a+b+c)\}Ge_3 \to Ge_4 \qquad & e_z(Ge_3) = e_z(Ge_4)e^{-i\pi\delta} \end{aligned}$$

where the eigenvector components transform according to $\{R|v\}\{e\} = \{e\}\chi^j(R)e^{-2\pi i q \cdot v}$. There, $\{R|v\}$ is a symmetry operation, $\{e\}$ is the set of all eigenvector components and $\chi^j(R)$ is the character belonging to the operation R for the jth irreducible representation (see table 1).

In order to relate the AMFs of Ge_1 and Ge_3, i.e. the quantities $u(t, Ge_1)$, $u(t, Ge_3)$, the generally valid relation

$$e(-q) = e(q)^*$$

is used, where the star denotes the complex conjugate. Under the inversion $\{I|0\}$ the Ge_4 atom at $-a-b$ is mapped onto Ge_1, which corresponds to choosing the origin at $q \cdot t = 0$, i.e.

$$\begin{aligned} \{I|0\}(ce_z(Ge_4)e^{i2\pi q(-a-b)}) &= -ce_z(Ge_3)e^{i\pi\delta}e^{i2\pi q(-a-b)} = -ce_z(Ge_3)e^{-i\pi\delta} \\ &= ce_z^*(Ge_1) \Leftrightarrow e_z(Ge_3) = -e_z^*(Ge_1)e^{i\pi\delta}. \end{aligned}$$

Thus, evaluation of the expression of $u(t, \mu)$ for the Ge atoms leads to the AMFs

$$\begin{aligned} u(t, Ge_1) &= c\varepsilon_{Ge}\cos(2\pi q \cdot t + \Theta_{Ge}) \\ u(t, Ge_2) &= c\varepsilon_{Ge}\cos(2\pi q \cdot t + \Theta_{Ge} + \pi\delta) \\ u(t, Ge_3) &= -c\varepsilon_{Ge}\cos(2\pi q \cdot t - \Theta_{Ge} + \pi\delta) \\ u(t, Ge_4) &= -c\varepsilon_{Ge}\cos(2\pi q \cdot t - \Theta_{Ge} + 2\pi\delta) \end{aligned} \tag{2}$$

where the complex component $e_z(Ge_1)$ has been split up into an amplitude and a phase factor according to $e_z(Ge_1) = e_z(Ge) = \varepsilon_{Ge}e^{i\Theta_{Ge}}$.

Similarly, Ge_1 and Ge_3 can be related by choosing $\{\sigma_y|\frac{1}{2}(a+b)\}$ to set the origin of $q \cdot t$ and to lock in the modulation. Under $\{\sigma_y|\frac{1}{2}(a+b)\}$, Ge_1 is mapped onto Ge_3, and the AMFs deduced from evaluating $u(t,\mu)$ fulfil the symmetry condition when applying an origin shift of $q \cdot t \rightarrow q \cdot t + \Delta$, with $\Delta = \frac{1}{4}(1-\delta)$. The AMFs then read

$$\begin{aligned}
u(t, Ge_1) &= c\varepsilon_{Ge} \cos\left(2\pi q \cdot t + \frac{\pi}{2} - \frac{\delta\pi}{2} + \Theta_{Ge}\right) \\
u(t, Ge_2) &= c\varepsilon_{Ge} \cos\left(2\pi q \cdot t + \frac{\pi}{2} - \frac{\delta\pi}{2} + \Theta_{Ge} + \pi\delta\right) \\
u(t, Ge_3) &= -c\varepsilon_{Ge} \cos\left(2\pi q \cdot t + \frac{\pi}{2} - \frac{\delta\pi}{2} - \Theta_{Ge} + \pi\delta\right) \\
u(t, Ge_4) &= -c\varepsilon_{Ge} \cos\left(2\pi q \cdot t + \frac{\pi}{2} - \frac{\delta\pi}{2} - \Theta_{Ge} + 2\pi\delta\right).
\end{aligned} \tag{3}$$

Equations (2) and (3) are fully equivalent representations of the AMFs for δ being irrational (i.e. q being incommensurate) and different from zero. For $\delta \rightarrow 0$, however, this AMF origin choice becomes significant and determines the resultant space group symmetry of the low-symmetry phase, i.e.

$P2_1/n11$ for origin choice $\Delta = 0$

$Pna2_1$ for origin choice $\Delta = \frac{1}{4}$.

We conclude that the *same* eigenvector $e(q, Ge)$ results in different subgroups of *Pnam* for different choices of the origin of $q \cdot t$. These space groups not only comply with the Bravais lattices observed in the low-symmetry ε-phase but are also in accordance with the systematic extinction conditions revealed by precession photographs, which were recorded in the ε-phase.

It was already pointed out in subsection 4.2 that TGC is a very soft material. The exact relationship between the order parameters and the free energy will, therefore, be very sensitive to external and internal stresses resulting from pressure, defects and, especially, internal surfaces imposed by the formation of ferroelastic domains (see subsection 4.2). Such domain walls imply high local stresses. An accurate phenomenological description has to take into account an elastic interaction of the stress field with the strain (see Salje 1990, ch 7). However, in terms of the simple free energy potential (1), it might be assumed that α becomes critical in the unstressed regions, whereas α' does so in the stressed regions, i.e. near the domain walls.

4.3.1. The nature of the order parameters ξ and η. The order parameters ξ and η can be related to two different contributions of the displacive modulation, i.e. a translational and a rotational 'motion' of the $GeCl_3$ molecule and, similarly, of the TMA molecule. However, ξ and η are not just identical with either of these two 'motions'.

The amplitudes of the AMFs of, for example, the Ge and Cl atoms resulting from the refinement of the incommensurately modulated structure (Fütterer *et al* 1995) can be interpreted in terms of a rigid-body translation and rotation of the $GeCl_3$ molecule. The rotation axis is assumed to coincide with the Ge atom and to be perpendicular to the plane defined by the three chlorine atoms (see figure 9). The difference of the z amplitude of Ge (0.419 Å) on the one side and Cl1 (0.358 Å), Cl2 (0.546 Å) on the other side is in agreement with a rotation about this axis of ~3.63°. Similarly, the x and y amplitudes of Cl1 (0.085 Å, 0.077 Å) would correspond to a rotation angle of 3.87°. The AMFs of

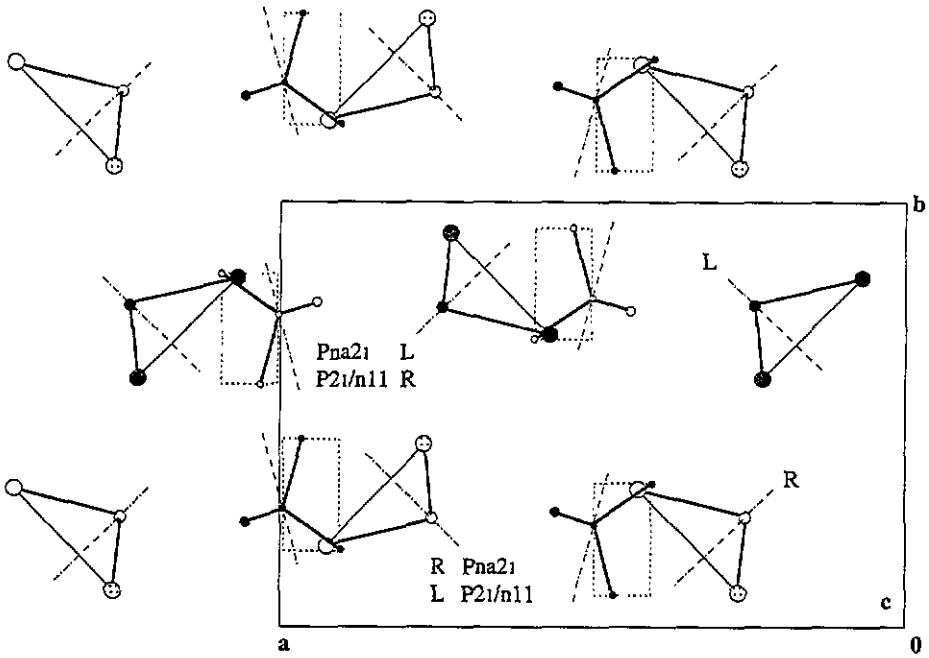

Figure 9. Projection of the average structure of δ-TGC down c. The $GeCl_3$ and the TMA molecule are represented by larger and smaller circles, respectively. The dashed rectangle indicates the atoms N, C1, C2 situated on the m_z mirror, while the atom C3 is off plane and on top of the m_z-related C3′. Similarly, $GeCl_3$ is represented by Ge and Cl2 (both in plane) and Cl1 (shaded, off plane), the latter being on top of the m_z-related Cl1′. The rotation axes of the molecules are also situated in the m_z mirror plane and are indicated by a dashed–dotted line with R and L denoting right- and left-hand rotation, respectively. Molecules drawn with closed and open circles are situated on the m_z mirror at $z = \frac{1}{4}$ and $z = \frac{3}{4}$, respectively.

N and C1, C2 and C3 could be interpreted in the same way, resulting in a rotation of the TMA molecule of 14.66° . The rotation axis in this case is defined by the nitrogen atom, the m_z mirror plane and an inclination angle of 10° to the *b* axis (see figure 9). In fact, the above interpretation was confirmed by a new refinement of the modulated structure in terms of rigid-body translational (along **c**) and rotational displacements of both the $GeCl_3$ and the TMA molecule giving rotation angles of 4.15° and 13.87° , respectively (Fütterer, unpublished results).

The translational displacements along *c* associated with the $Pna2_1$ and the $P2_1/n$ modes for $q = 0$ can be easily deduced from the expressions (2) and (3) (see figure 10). A displacement $+z_0$ is assumed for the $GeCl_3$ molecules situated at $x = \frac{1}{4} \pm \varepsilon$ (figure 10, (i)). The adjacent TMA molecules at $x = 0.5$ and $x = 0.0$ are in phase to the $GeCl_3$ molecules at $(x, y, z) = (\frac{1}{4}, \frac{1}{4}, \frac{3}{4})$ and $(\frac{1}{4}, \frac{3}{4}, \frac{1}{4})$, respectively (note that the $GeCl_3$ and TMA molecules, which are in phase, overlap in the projection along *c* in figure 9). The $P2_1/n$ mode would result in a displacement $-z_0$ for the $GeCl_3$ molecules situated at $x = \frac{3}{4} \pm \varepsilon$ (figure 10, (iib)) implying that $\{\sigma_y|\frac{1}{2}(a+b)\}$ is not preserved. We shall call this the $(+z_0, -z_0)$ displacement pattern. (Note that the $GeCl_3$ molecules at $x = \frac{1}{4} \pm \varepsilon$ and at $x = \frac{3}{4} \pm \varepsilon$ are related by symmetry operations, which map q onto $-q$.) By way of contrast, the $Pna2_1$ mode results in a displacement $+z_0$ for the $GeCl_3$ molecules at $x = \frac{3}{4} \pm \varepsilon$ (figure 10, (iia)), labelled $(+z_0, +z_0)$. Obviously, the $(+z_0, +z_0)$ displacement pattern not only preserves $\{\sigma_y|\frac{1}{2}(a+b)\}$, but would still allow $\{\sigma_z|\frac{1}{2}c\}$ to hold. However, the polarity implied by

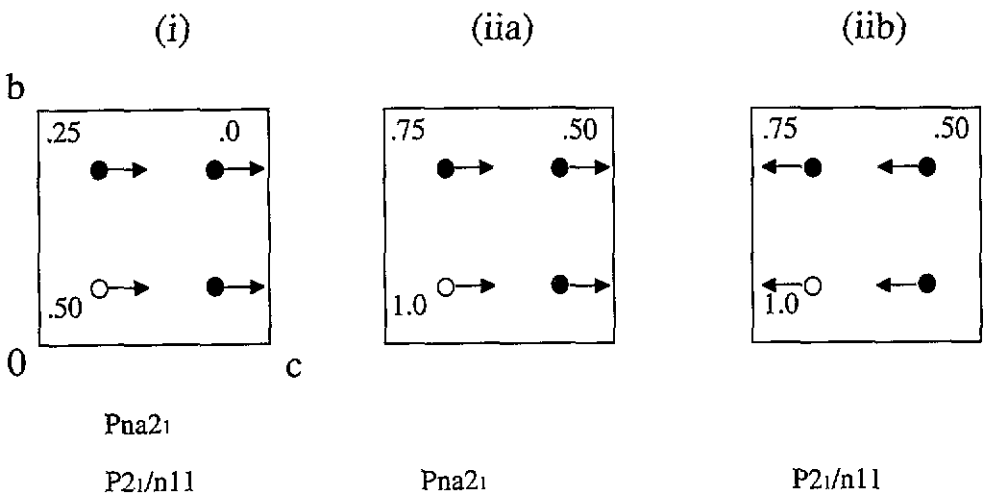

Figure 10. Schematic representation of the translational part of the displacive modulation of the δ-phase at the lock-in $q \to 0$. Given a displacement $+z_0$ of the $GeCl_3$ molecules at $x = \frac{1}{2} \pm \varepsilon$ (i), the resulting displacements of the molecules at $x = \frac{3}{4} \pm \varepsilon$ corresponding to the $Pna2_1$ and the $P2_1/n11$ mode are shown in (iia) and (iib), respectively. Shaded circles represent the $GeCl_3$ molecules, while open and closed circles represent TMA molecules, which are in phase to the adjacent $GeCl_3$ molecule, at different heights in x. The latter are indicated by (approximate) fractional coordinates.

$Pna2_1$ space group symmetry is provided for by the rotational displacement, which is, of course, incompatible with the m_z mirror plane.

It is obvious from the expressions (2) and (3) that the $(+z_0, +z_0)$ and the $(+z_0, -z_0)$ displacement patterns are 90° out of phase (in the limit $\delta \to 0$), analogous to the second solution of the free energy potential (1) (and analogous as well to the Ψ and Φ modes of the McConnell–Heine model, Heine and McConnell 1984). Yet these two displacement patterns cannot be directly identified with the order parameters ξ and η, because the rotational displacement pattern has also to be included. From the structure refinement mentioned above, the rotational and translational contributions were shown to be approximately (but not exactly) 45° out of phase. This implies that rotational 'motion' contributes to both ξ and η.

4.4. Relationship between disorder in the γ-phase and the displacive modulation in the δ-phase?

The presence of short-range disorder in the γ-phase is revealed by the observed diffuse x-ray scattering displayed in figure 4. A pattern with the characteristics as described under item (3), 3.1, requires transverse 'motion' along both the [010] and [001] directions, i.e. $F(G+q) \propto (G+q) \cdot e(q)$, where F is a structure factor, G a reciprocal Bravais lattice vector, q the wave vector of the phonon mode and e its eigenvector.

The observation of this diffuse streaking is in agreement with the finding of unusually high thermal parameter tensor components U_{ii} in the γ-phase. Moreover, not only is U_{33} distinctly higher than U_{11} and U_{22}, but a plot of U_{ii} versus temperature shows that U_{11}, U_{22} extrapolate to zero for $T \to 0$, whereas U_{33} does not (see figure 2, adapted from Hesse *et al* 1995). This may suggest that the high values of U_{33} result from disorder rather than pure thermal motion.

The correspondence in orientation of U_{33} in the γ-phase and of the major modulation amplitude in the δ-phase (item (2), subsection 3.3) suggests a relationship between the structural disorder in the γ-phase and the incommensurate modulation of the δ-phase.

The example of α-PbO (litharge) suggests, furthermore, that the diffuse streaks observed in γ-TGC might be a precursor to the formation of satellite reflections at $\sim$0.14 b^*. Transmission electron microscopy (TEM) of lead oxide samples revealed the presence of analogous diffuse streaks along $[110]_t^*$ and $[1\bar{1}0]_t^*$ (Wang *et al* 1992, Withers *et al* 1993; the subscript t refers to the tetragonal axes). Those diffuse streaks were observed to transform into satellite reflections located at $\sim$ 0.185 $(-a_t^* + b_t^*)$ and occurring below $T_c = 228$ K owing to the normal–incommensurate phase transition in α-PbO (Withers *et al* 1993, Le Bellac 1993). The analogy between those two compounds is supported by the structural similarity of their incommensurate phases with regard to the presence of one predominant, shear-wave-like modulation amplitude (Le Bellac 1993).

The strikingly different behaviour of lattice parameter a compared to b and c at and below $T_{\gamma-\delta}$ would also become plausible, given the above-proposed relationship. The γ–δ phase transformation would then be linked to the transition from uncorrelated 'motion' (i.e. short-range disorder in γ-TGC) to correlated 'motion' (i.e. the displacive modulation in δ-TGC) at the γ–δ transition, as will be outlined subsequently: it was shown (Fütterer *et al* 1995) that the average structure of δ-TGC and also (because it is isomorphous to the former) the structure of γ-TGC could be regarded as being built up of sheets of $GeCl_3$ and TMA molecules. Those sheets are oriented perpendicular to, and alternately stacked along, the a axis. The major modulation wave amplitude is oriented within these sheets, as is apparently (indicated by $U_{33} > U_{11}, U_{22}$) the main displacement associated with the disorder. Thus, with decreasing temperature the sheets get closer to each other as a contracts. At the γ–δ transition they get into 'contact', marked by the drastic change of the slope $\partial a/\partial T$. This 'contact' might, on the one hand, couple the 'motion' of adjacent sheets, while inhibiting a further contraction of a on the other hand.

The data resulting from the refinement of the incommensurate structure (Fütterer *et al* 1995, see figure 2) suggest that short-range disorder disappears only in the ε-phase and point to a possible superposition of disorder and displacive modulation in the δ-phase. In conclusion one can say that, though there are strong indications in favour of the relationship discussed above, unequivocal experimental confirmation is still required.

5. Conclusion

To summarize our results we would like to emphasize the following points. First, the modulation of the incommensurate δ-phase is most appropriately described as being composed of a translational displacement along c coupled with a rotation of the otherwise rigid $GeCl_3$ and TMA molecules. The translational and rotational parts are approximately 45° out of phase. Secondly, two order parameters, ξ and η, obeying two different irreducible representations (at $q = 0$) can interact via a gradient coupling term in a simple Landau potential. This free energy potential, expanded in terms of ξ and η, can account for the occurrence of the modulated phase as well as for the two coexisting Bravais lattices in the ε-phase. The order parameters can be related to translational displacement patterns $(+z_0, -z_0)$ and $(+z_0, +z_0)$ of subsequent sheets of $GeCl_3$ molecules corresponding to $P2_1/n11$ and $Pna2_1$ modes, respectively. The rotational part contributes to both order parameters and especially accounts for the polar axis in $Pna2_1$. Thirdly, the observation of two coexisting Bravais lattices in the ε-phase is attributed to a ferroelastic domain pattern with monoclinic domains separated by orthorhombic domain boundary regions. This is

based on the experimental observation via polarized light microscopy of such a domain pattern and on the low bulk modulus of the material. We presume this low bulk modulus allows a smooth transition zone between adjacent monoclinic domains.

However, there remain some points still to be understood and to be examined in further detail—particularly the temperature dependence of the intensity ratio of monoclinic and orthorhombic reflections in the ε-phase. A more detailed examination of the ferroelastic domain pattern with polarized light microscopy would obviously be of interest. Furthermore, the assumed relationship between short-range disorder in the room-temperature phase and the displacive modulation in the incommensurate phase still needs unequivocal experimental confirmation. A corresponding investigation of the temperature-dependent behaviour of the diffuse x-ray scattering is currently under way.

Acknowledgments

We are indebted to Drs R Loucks and M Shelley from Research School of Earth Sciences, ANU, for their support in carrying out the polarized light microscopy experiment. Also, we would like to thank Dr. Sherry Mayo for sample preparation for the diffuse scattering experiments as well as H H Eulert and Dr K F Hesse for their support in carrying out the low-temperature single-crystal x-ray diffraction experiments. The Guinier powder diffactometer was made available by the Deutsche Forschungsgemeinschaft under contract No DE 412-1/2.

References

Dolino G 1986 *Incommensurate Phases in Dielectrics—2. Materials* ed R Blinc and A P Levanyuk (Amsterdam: Elsevier) pp 205–32

Fütterer K 1994 *PhD Thesis* Technical University Berlin

Fütterer K, Depmeier W and Petříček V 1995 *Acta Crystallogr.* B at press

Heine V and McConnell J D C 1984 *J. Phys. C: Solid State Phys.* **17** 1199–220

Hensler J, Boysen H, Bismayer U and Vogt T 1993 *Z. Kristallogr.* **206** 213–31

Hesse K F, Eulert H H and Depmeier W 1995 personal communication

Hovestreydt E, Aroyo M, Sattler S and Wondratschek H 1992 *J. Appl. Crystallogr.* **25** 544

Le Bellac D 1993 *PhD Thesis* Université Paris-Sud

Levanyuk A P 1986 *Incommensurate Phases in Dielectrics—2. Materials* ed R Blinc and A P Levanyuk (Amsterdam: Elsevier) pp 1–41

Levanyuk A P and Sannikov D G 1976 *Sov. Phys.–Solid State* **18** 1122–25

Majkrzak C F, Axe J D and Bruce A D 1980 *Phys. Rev.* B **22** 5278–83

Mashiyama H 1981 *J. Phys. Soc. Japan* **50** 2655–9

Möller A 1980 *PhD Thesis* University Konstanz

Osborn J C and Welberry T R 1990 *J. Appl. Crystallogr.* **23** 476–84

Rabe H and Schmid H 1993 *Ferroelectrics* **161** 49–54

Salje E K H 1990 *Phase Transitions in Ferroelastic and Co-elastic Crystals* (Cambridge: Cambridge University Press)

Sciau P, Calvarin G, Sun B and Schmid H 1992 *Phys. Status Solidi* **129** 309–21

Wang Y G, Ye H G, Kuo K H and Guo J G 1992 *J. Appl. Crystallogr.* **25** 199–204

Withers R L, Schmid S and Fitz Gerald J D 1993 *Defects and Processes in the Solid State: Geoscience Applications—The McLaren Volume* ed J N Boland and J D Fitz Gerald (Amsterdam: Elsevier) pp 305–16

Yamada K, Isobe K, Okuda T and Furukawa Y 1994 *Z. Naturf.* a **49** 258–66